Numerical and Analytical Modelling of Hat-section Web Crippling Behaviour

References

[1] *ENV 1993-1-3 Design of steel structures*, Part 1-3 Supplementary rules for cold formed thin gauge members and sheeting, ECS, 1996

[2] RECK, P. – PEKÖZ, T. – WINTER, G.: *Inelastic strength of Cold-Formed Steel Beams*, J. of Structural Division, ASCE, No. 11/1975

[3] VRANÝ, T.: *Thin-walled cold-formed Z-purlins, in Steel Structures*, Dpt. Of Steel Structures, CTU, 1998 (in Czech)

[4] TOMA, T. – WITTEMAN, K.: *Design of Cold-Formed Purlins and Rails Restrained by Sheeting*, J.Construct. Steel Research Vol. 31, No. 2–3, 1994

Received: 1999.06.23

Tomáš Vraný,
CTU, Dept. of Steel Structures,
Thákurova 7, 166 29 Prague 6,
Czech Republic

NUMERICAL AND ANALYTICAL MODELLING OF HAT–SECTION WEB CRIPPLING BEHAVIOUR

H. HOFMEYER, J. G. M. KERSTENS, H. H. SNIJDER, M. C. M. BAKKER

Key words: Hat-sections, Thin-Walled Steel, Web Crippling, Analytical Modelling, Numerical Modelling.

Hat-sections of thin-walled steel are subject to a concentrated load and a bending moment at an interior support. For a large concentrated load and a small bending moment, two failure mechanisms can occur: the yield-arc and the rolling mechanisms. Research indicated that the corner radius has a strong influence on the failure mechanism to occur [1-2]. It has been investigated whether small strips of the hat–section cross-sections can be used to gather insight into the differences of the two failure mechanisms. For small corner radii, strip behaviour and section behaviour are comparable. For large corner radii, this is not the case. Finite element models have been used to describe the cross-sectional behaviour of hat–sections for varying corner radii. Relatively simple analytical models have been derived which determine the location of first yield in the cross-section's web and the cross-section's rigid-plastic behaviour. Except for the largest corner radius, analytical models and finite element models give comparable results.

1. Introduction

Thin-walled steel sheeting is frequently used for cladding and roof construction. To test the sheeting's resistance to combined bending moment and concentrated load, often hat–sections are used instead of sheeting in a three point bending test, figure 1.

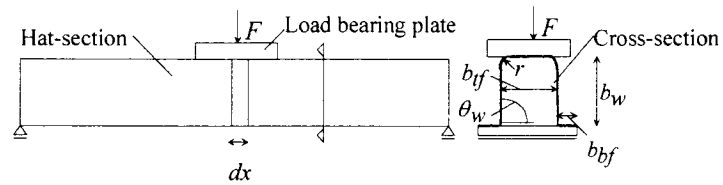

Figure 1: Three point bending test of a hat-section, the cross-section defines some variables.

These three point bending tests indicate that hat-sections subjected to a large concentrated load and a small bending moment can fail by two failure mechanisms: the rolling and the yield-arc mechanisms, figure 2. Bakker [1] studied the rolling and yield-arc mechanisms and some related observations are presented in the next paragraph.

1.1 Rolling and Yield-arc Failure Mechanisms

Bakker [1] found that one very important section variable which determines whether the yield-arc or rolling mechanism occurs is the section corner radius (r in figure 1).

Web crippling deformation is defined as the decrease of cross-section height below the load bearing plate. This is shown in figure 2 at the left. The rolling and yield-arc mechanisms each have a characteristic load-deformation curve as shown in figure 2 at the right.

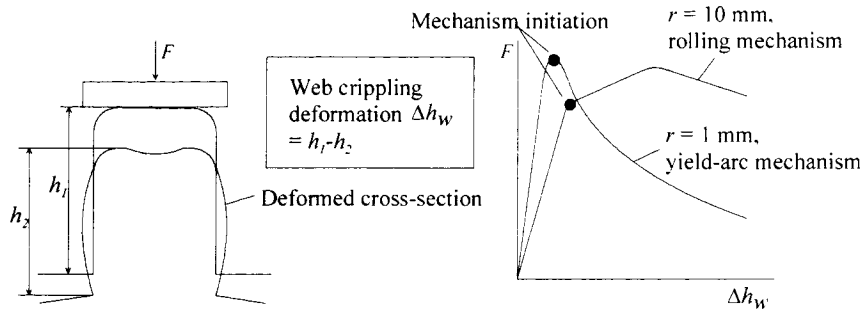

Figure 2: Qualitative load-web crippling behaviour for rolling and yield-arc mechanisms.

Before both mechanisms initiate, the hat-sections first behave elastically: the straight lines in the load-web crippling deformation curves. Thereafter, the failure mechanism initiates and plasticity occurs. The initiation of the failure mechanism is marked with a bold dot for both mechanisms (the mechanism initiation points). After mechanism initiation, the rolling mechanism increases in strength. After some deformation, the strength reduces. The yield-arc mechanism decreases in strength immediately after mechanism initiation.

Figure 3 shows the yield line patterns of the two failure mechanisms. A rolling mechanism (figure 3 at the top) starts with the moving yield lines 7 and 8 near the upper corner. For an increase of the load, the moving yield line 8 in the web moves downward in the web. The moving yield line 7 in the top flange moves through the corner. After further increase of the load, other yield lines (1 to 6) will occur in the flange and web for reasons of compatibility. A yield-arc mechanism (figure 3 at the bottom) starts with the curved yield line 8 in the web. For an increase of the load, the movement of this yield line is negligible small. As for the rolling mechanism, other yield lines (1 to 7) will occur for reasons of compatibility after some loading.

1.2 Cross-sectional Behaviour

Bakker introduced the rolling and yield-arc mechanisms by simple mechanical models as shown in figure 4. Yield line numbers are according to figure 3.

For the longitudinal section, the rolling and yield-arc mechanisms are quite similar: yield lines 1 to 6 are all fixed and have more or less the same positions for the rolling and yield-arc mechanisms in figure 3. Thus, only one simple mechanical model for the longitudinal section is used in figure 4. For the cross-section the rolling and yield-arc mechanism are different: yield lines 7 and 8 are moving for the rolling mechanism, but fixed for the yield-arc mechanism. Thus, two simple mechanical models are used for the cross-sectional behaviour in figure 4.

The simple mechanical models in figure 4 suggest that the differences between the two failure mechanisms may be explained by investigating the differences of the mechanisms for the cross-section only.

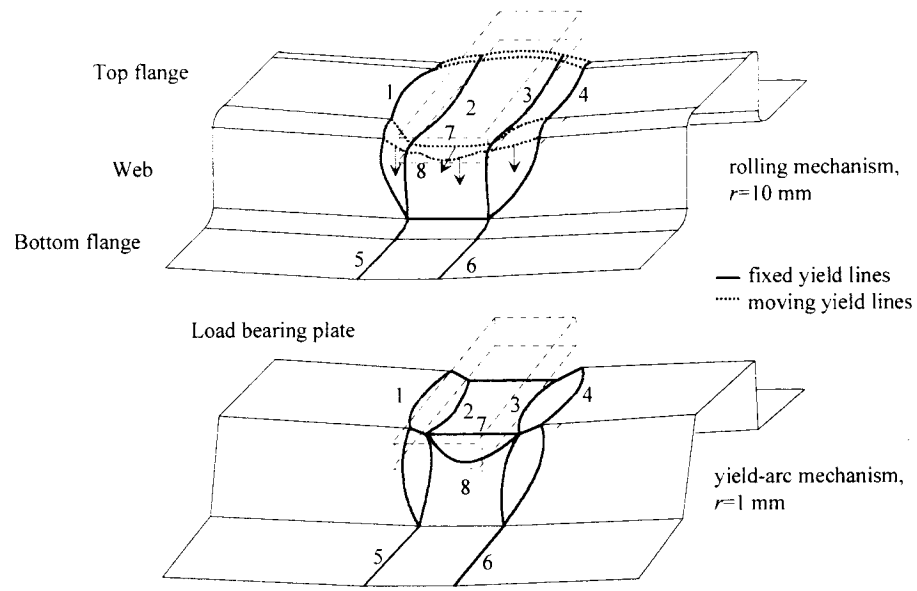

Figure 3: Rolling and yield-arc mechanisms.

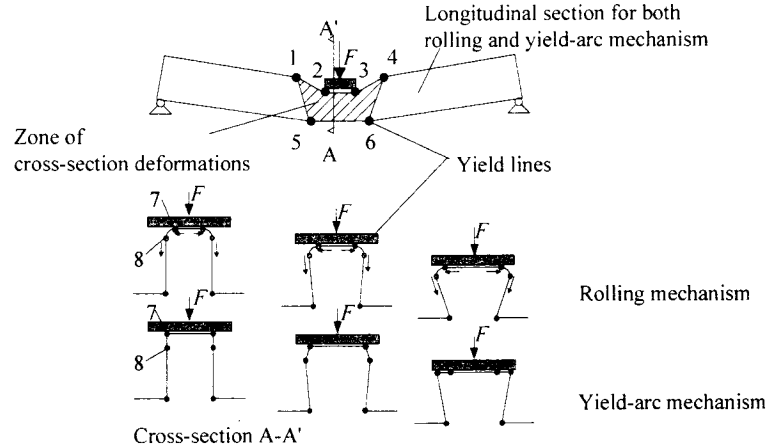

Figure 4: Rolling and yield-arc mechanisms presented by simple mechanical models [1].

For this reason, only the cross-sectional behaviour of hat-sections is investigated in this paper. With the finite element method, a small strip dx of the hat-section as shown in figure 1 is modelled. The simulations are presented in section two. For the same strip dx, an analytical model has been derived. This model makes it possible to predict the behaviour of the two failure mechanisms for the strip dx. The analytical model is presented in section

three. Chapter 4 presents a comparison between the analytical model of section three and an already existing model and a comparison of finite element models for a strip dx and whole hat-sections.

2. Numerical Simulations

2.1 Support Conditions

In the previous section, it was explained that the cross-sectional behaviour of hat-sections would be studied by the behaviour of a strip dx of the hat-section. Normally, this strip dx is kept in place by the flanges and web adjacent to the strip. Without these adjacent parts, the strip dx should be fixed into space to make loading possible. It can only be fixed at the bottom because otherwise, cross-sectional deformations will not be possible. Figure 4 shows that for the cross-section, the bottom flange and bottom corner do not play a significant role in the cross-sectional behaviour. Therefore, the bottom flange and bottom corners are not modelled in the numerical model. Regarding the possible rotation of the bottom of the web, due to all sort of actions of the neglected bottom flange and corner, two extreme situations are modelled: hinged and clamped.

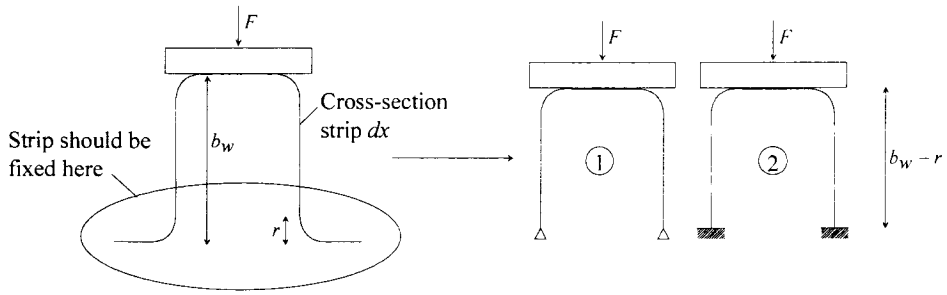

Figure 5: Two possibilities to fix the strip dx: hinged and clamped.

2.2 Finite Element Model

Figure 6 presents a finite element model for the strip dx. At the top of the figure, the load bearing plate is shown. This plate is modelled as a solid piece of steel. Load is applied by a forced displacement of the load bearing plate along the negative y-axis. Contact elements are modelled between the load bearing plate and the top flange to prevent penetration of the load bearing plate into the strip. A geometrically non-linear analysis has been carried out, accounting for small strains and large rotations.

Elements sizes are 3 × 3 mm for web and top flange. The corner is modelled by 10 elements. Shell elements are used, having four nodes with six degrees of freedom each and five integration points along the thickness. The material behaviour is given by points of the stress-strain curve of the steel used. Plasticity and hardening is thus taken into account. Some variables of the steel used are: yield strength 335 [N/mm^2], modulus of elasticity 210.000 [N/mm^2], strain at yielding 0.003 [1].

Boundary conditions are shown in figure 6. The two sides of the strip (for which $z = 0$ and 3 mm) are part of a symmetry surface. This is also true for the nodes at the top flange edge.

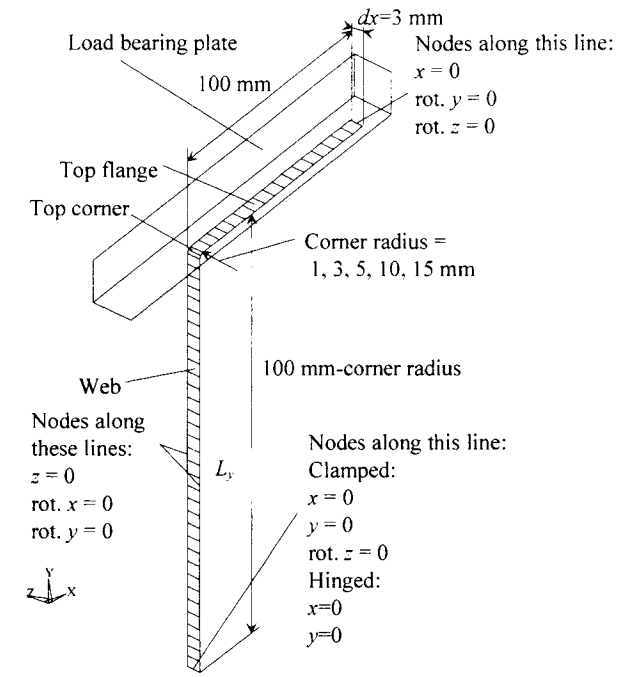

Figure 6: Finite element model.

Because of these symmetry conditions, the strip width is not of importance. The strip width of the model is chosen arbitrarily to be $dx = 3$ mm. Nodes at the bottom of the web corner are fixed for movement along the $x-$ and $y-$axis. The rotation around the $z-$axis is free or fixed for a hinged or clamped condition.

Results of the simulations are interesting for two main aspects. Load-deformation behaviour (paragraph 2.3), and location and movement of the first yield line (paragraph 2.4).

2.3 Load-deformation Behaviour

Paragraph 1.1 presented web crippling deformation, and load-deformation curves for the rolling and yield-arc mechanisms for hat-sections.

Figure 7 presents the load-deformation curves for the strips of the finite element models. From r=1 mm to r=10 mm, the qualitative behaviour of the strip dx is the same for the hinged and clamped situation. However, the ultimate loads are higher for the clamped situation. For r=15 mm, the clamped situation leads to an ascending curve after elastic behaviour. In the next paragraph, it is shown that an additional yield line occurs for r=15 mm. This difference can cause the ascending curve for r=15 mm.

If the curves at the right in figure 2 and figure 7 are compared, it can be seen that for r=1 mm the load-deformation curves are qualitatively similar for both figures. For r=10 mm, the curves are qualitatively different. Figure 2 shows an ascending curve after mechanism

initiation and hereafter a descending curve. Figure 7, however, shows a descending curve directly after elastic behaviour. This means that for r=10 mm, the cross-sectional behaviour according the finite element model, cannot be used to explain the ascending curve in the three-point bending tests.

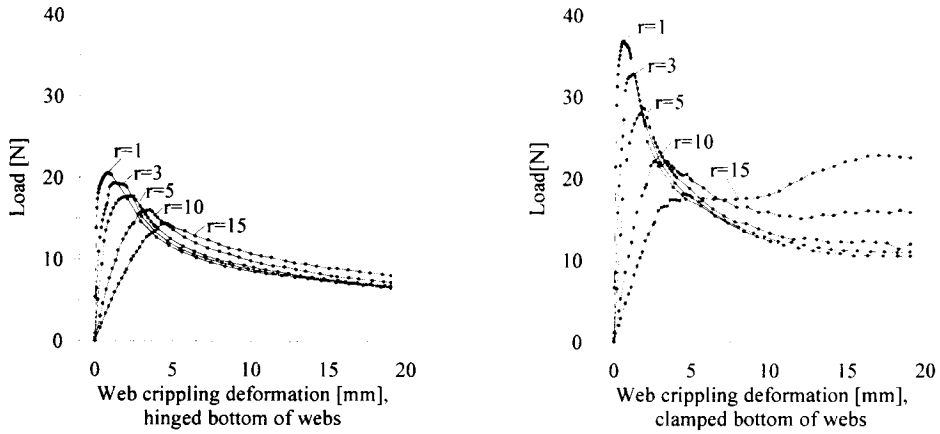

Fig. 7: Load-deformation curves for finite element models for different corner radii, hinged bottom of webs at the left, clamped bottom of webs at the right.

Looking at all curves for all corner radii in figure 7, it seems that there is not really a typical curve for the yield-arc (r=1 mm) or the rolling (r=10 mm) mechanism, but that there is a smooth transition between all the curves. In the next paragraph, it will be shown that for the location and movement of yield lines, an equivalent transitional behaviour occurs.

2.4 Location and Movement of the First Yield Line

A yield line will occur in the web as shown in figure 8 with a continuous bold line. During further deformation this yield line will move downwards in the web. Figure 8 defines the initial position (L_y), the movement direction (arrow), and distance moved (d_y) of the yield line. After the forming of a yield line in the web, yield lines will occur in the top flange (dotted in figure 8) and at the bottom of the web for clamped bottoms of the web. For r=15 mm, for clamped bottoms of the web, an additional yield line occurred in the top corner, also dotted in figure 8. This yield line in the top corner may cause the different load-deformation behaviour for r=15 mm. All yield lines contain significantly smaller plastic strains than the main yield line in the web and therefore they will not be subject to further investigation in this paragraph.

Table 1 presents the distance L_y for r=1 mm to r=15 mm for hinged and clamped bottoms of the web. For clamped bottoms of the web, for r=10 mm, the yield line in the web is located almost at the top corner. For r=1 mm, the yield line is located above the middle in the web. This is also true for three-point bending tests (see figure 3). For hinged bottoms of the web, the yield line in the web is located approximately in the middle for all corner radii r. From now on, only the model with clamped bottoms of the web will be used, because this model has more similarities with full three-point bending tests.

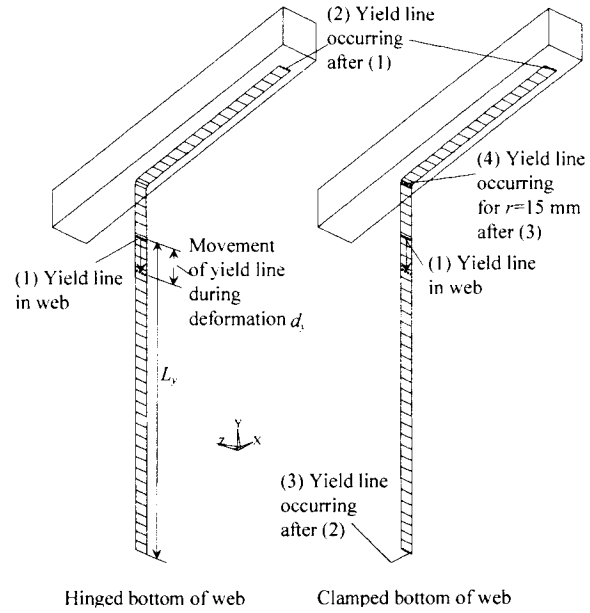

Figure 8: Location of yield lines.

Figure 9 presents yield line position L_y and yield line movement d_y for r=1 mm to r=15 mm for clamped bottoms of the web.

As figure 9 shows in the left graph, the yield line is located lower if the corner radius is smaller. Because the graph presents the yield line position as function of the web crippling deformation, it can be seen that for increasing deformation, the yield lines move. This is true for all corner radii. The graph at the right presents the movement of the yield lines d_y. In general, yield line movement increases for larger corner radii. As an exception, for a corner radius equal to 15 mm, the yield lines moves comparable to r=1 mm and r=3 mm. This may be an indication that for r=15 mm another failure mechanism occurs. This indication is strengthened by the occurrence of an extra yield line in the top corner for r=15 mm.

r [mm]	L_y [mm] hinged bottoms of the web	L_y [mm], clamped bottoms of the web
1	46.0	64.3
3	47.0	66.2
5	49.4	69.8
10	56.5	80.0
15	61.3	72.5

Table 1: distance L_y for all simulations at mechanism initiation.

In paragraph 1.2, it was mentioned that for whole hat-sections, moving yield lines exist for the rolling mechanism (r=10 mm) and fixed yield lines exist for the yield-arc mechanism

(r=1 mm). Figure 9 points out that for r=1 mm the yield line in the web indeed is almost fixed in position and that for r=10 mm the yield line is moving strongly.

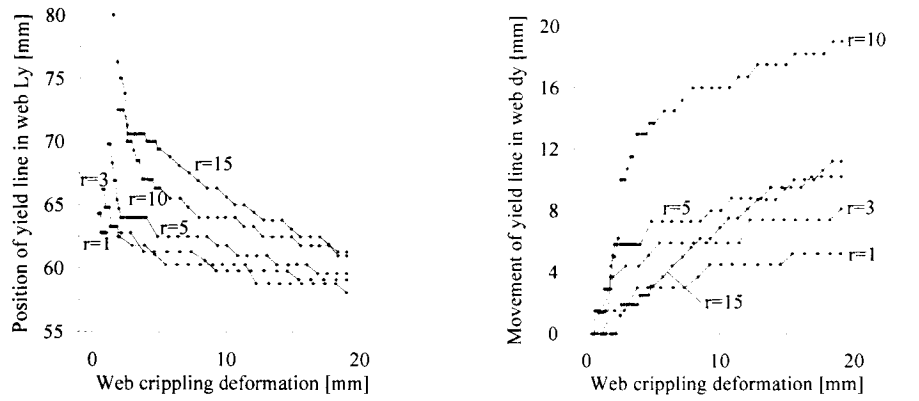

Fig. 9: Location and movement of yield lines. At the left yield line position L_y and at the right yield line movement d_y.

3. Analytical Model

For describing the behaviour of a small strip dx of the hat-section, an analytical model has been developed. First, the location of the first yield line in the web is determined by calculating the maximum bending moment in the web. Then, an analytical model is presented in paragraph 3.2, which predicts the rigid-plastic behaviour of the strip.

3.1 Location of First Yield

The geometry for the calculation of the ultimate bending moment in the web is shown in figure 10.

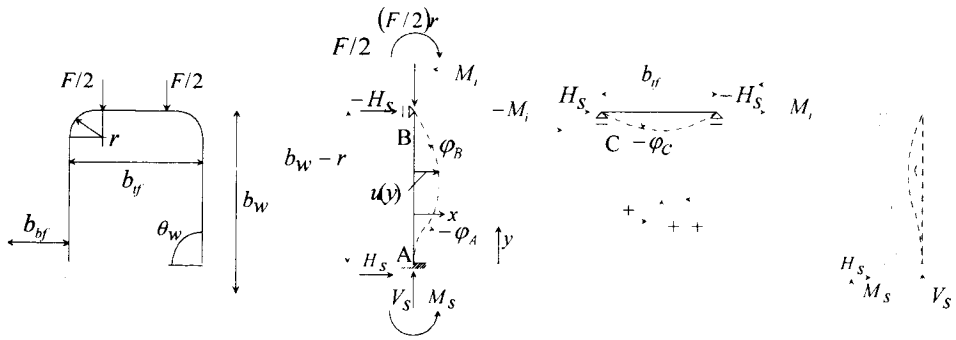

Figure 10: Cross-section and simplified cross-section of strip dx.

At the left of figure 10, the cross-section of the strip dx is shown. The load bearing plate and the load F acting on this plate have been replaced by two forces $F/2$ at the intersection of the top corners and the top flange. This is acceptable because if the cross- section is loaded, it will deform as shown in figure 2 at the left. Then, the load bearing plate only contacts the intersections of top corners and top flange. The cross-section at the left is simplified at the right side of the figure. The bottom flange has been removed, as for the finite element models in section two. The corner radius has been flattened. Instead of the force $F/2$ having a distance r to the web in horizontal direction, the load is applied directly on the web plus an additional bending moment $(F/2)r$. Because the strip dx is symmetrical, the right web needs not to be modelled.

Now, the second-order bending moment in the web as a function of the distance y will be derived. The rotation at location C can be calculated by:

$$\varphi_C = \frac{M_i b_{tf}}{2EI} \tag{1}$$

Horizontal forces in the top flange are neglected because they will make the calculation very complex and the finite element models showed these forces to be very small compared to the Euler load of the top flange.

The second-order rotation at location B can be calculated by using equations for bending of prismatic bars presented by Timoshenko [3]:

$$\varphi_B = -\frac{M_S\,(b_w - r)}{6EI}\phi(\eta) - \frac{(F/2)r - M_i(b_w - r)}{3EI}\psi(\eta) \tag{2}$$

$$\phi(\eta) = \frac{3}{\eta}\left(\frac{1}{\sin(2\eta)} - \frac{1}{2\eta}\right). \tag{3}$$

$$\psi(\eta) = \frac{3}{2\eta}\left(\frac{1}{2\eta} - \frac{1}{\tan(2\eta)}\right). \tag{4}$$

$$\eta = \frac{b_w - r}{2}\sqrt{\frac{(F/2)}{EI}}. \tag{5}$$

The rotation at location C should be equal to the rotation at location B for which follows:

$$\frac{M_i b_{tf}}{2EI} = \frac{M_s(b_w - r)}{6EI}\psi(\eta) + \frac{(F/2)r - M_i(b_w - r)}{3EI}\varphi(\eta) \tag{6}$$

The rotation at location A should be zero and can be calculated by using the same equations for bars by Timoshenko [3]:

$$\varphi_A = 0 = \frac{((F/2)r - M_i)(b_w - r)}{6EI}\phi(\eta) + \frac{M_s(b_w - r)}{3EI}\psi(\eta) \tag{7}$$

Equation 6 and 7 can be solved to calculate the internal bending moment M_i and the reaction bending moment M_s:

$$M_i = (F/2)r\left(\frac{(b_w - r)\,(\phi^2(\eta) - 4\psi^2(\eta)}{\phi^2(b_w - r) - 6b_{tf}\psi(\eta) - 4(b_w - r)\psi^2(\eta)}\right) \tag{8}$$

$$M_s = (F/2)r\left(\frac{3b_{tf}\phi(\eta)}{\phi^2(b_w - r) - 6b_{tf}\psi(\eta) - 4(b_w - r)\psi^2(\eta)}\right) \tag{9}$$

If the two above presented moments are known, the displacement $u(y)$ of the web can be calculated, using equations presented by Timoshenko [3]:

$$u(y) = -\frac{M_s}{(F/2)}\left(\frac{\sin\left(\frac{2\eta}{b_w}y\right)}{\sin\left(\frac{2\eta}{b_w}b_w\right)} - \frac{y}{b_w}\right) + \frac{M_i - (F/2)r}{(F/2)}\left(\frac{\sin\left(\frac{2\eta}{b_w}(b_w - y)\right)}{\sin\left(\frac{2\eta}{b_w}b_w\right)} - \frac{b_w - y}{b_w}\right) \quad (10)$$

The horizontal reaction H_s can be calculated by described the moment equilibrium at the rigid support:

$$H_s = \frac{M_s + (M_i - (F/2)r)}{b_w - r} \quad (11)$$

The bending moment in the flange as a function of y can now be written as:

$$M(y) = M_s + H_s^{*}{}^{y} - (F/2)u(y) \quad (12)$$

Using the yield strength f_y and steel plate thickness t, the yielding moment of the strip d_x can be calculated by:

$$M_{pl} = \frac{2}{\sqrt{3}} * \frac{1}{4} * t^2 * f_y * d_x \quad (13)$$

Formula 13 has been derived by Hill [4]. Formula 12 is used to find the location of the yield line in the flange. Therefore, the next sequential steps will be followed:

1. A load $(F/2)$ is assumed. Formula 3, 4, 5, 8, 9, 11, and 12 can be used to calculate the bending moment $M(y)$ for a set of positions y. The maximum bending moment is the maximum value found for the set of positions.
2. The calculated maximum bending moment $M(y)$ is compared to the yielding bending moment of the strip M_{pl} (formula 13). If $M(y)$ is lower than M_{pl}, the assumed load $(F/2)$ should be higher. If $M(y)$ is greater than M_{pl}, the assumed load $(F/2)$ should be lower.
3. If the calculated value of the bending moment $M(y)$ equals the yielding moment M_{pl}, the load $(F/2)$ to initiate yielding in the flange has been found.

The above-presented sequence is carried out for a strip dx for five different corner radii: 1, 3, 5, 10, and 15 mm. The width of the strip equals 3 mm thus making possible a comparison between this model and the finite element models. Table 2 presents the results.

	Location L_y [mm] for maximum bending moment $M(y) = M_{pl}$		$(F/2)$ [N] for maximum bending moment $M(y) = M_{pl}$		$M(y) = M_{pl}$ [Nmm]
r [mm]	Analytical model	Finite element models	Analytical models	Finite element models	Both
1	61.9	64.3	36.5	36.5	138
3	64.7	66.2	31.4	31.7	138
5	67.1	69.8	27.4	25.8	138
10	73.1	80.0	19.8	15.9	138
15	80.2	72.5	14.2	11.0	138

Tab. 2: Initial position of the yield line in the web for strips dx, width 3 mm, having different corner radii.

There are some differences between the analytical model and the finite element model, but table 2 shows the analytical model gives a good indication of the location of first yield and the load $(F/2)$ at which first yielding occurs. Differences can be caused by:

1. The geometry of the analytical model is different from the geometry of the finite element model.
2. The analytical model predicts the location of the yield line by using the full plastic moment that occurs in the web, whereas the numerical model indicates first yield by (some) plastic strains in the outer fibres of the web.
3. In the analytical model, first order rotations are calculated for the top flange because the influence of the horizontal load in the top flange is not taken into account.

Table 3 presents the same five strips as in table 2, but now all are loaded by the same load $(F/2)$ equal to 10 N. The location of the maximum bending moment L_y and the value of the bending moment $M(y)$ are listed.

r [mm]	L_y for maximum $M(y)$ [mm]	$M(y)$ [Nmm]	$F/2$ [N]
1	94.6	6.1	10
3	94.0	18.6	10
5	93.4	31.3	10
10	90.0	64.5	10
15	85.0	99.5	10

Tab. 3: Results for constant load.

Table 3 shows that the location of the maximum bending moment comes down for an increasing corner radius r and fixed load $F/2$ (conclusion 1). The value of the maximum bending moment increases for an increasing corner radius (conclusion 2).

Table 4 presents the results for a strip having a corner radius r equal to 1 mm. The load is varied between 10 and 30 N.

Table 4 shows that for increasing load, the value of the maximum bending moment increases (conclusion 3) and the location of the maximum bending moment is lower (conclusion 4).

Using the four conclusions presented above, it can be explained why the yield line is located near the top corner for large corner radii and in the middle of the web for small corner radii.

r [mm]	x for maximum $M(y)$ [mm]	M_2 [Nmm]	$F/2$ [N]
1	94.6	6.1	10
1	82.7	9.7	15
1	75.4	15.0	20
1	70.2	24.0	25
1	66.1	42.3	30

Tab. 4: Results for constant corner radius.

If the corner radius r is small, a load results in a small moment $M(y)$ (conclusion 2). Therefore, the load $F/2$ has to be high to reach the yield bending moment (conclusion 3). If the load is high, the location of the maximum bending moment (and thus the yield line) is low (conclusion 4). These effects seems to be more important than the fact that the location of ultimate bending moment also decreases slightly for increasing corner radii (conclusion 1). For a large corner radius, the same conclusions can be used to show that the yield line occurs near the top corner.

A second-order calculation is needed to predict the position of the first yield line, as shown in figure 10 at the right. The reaction forces at the rigid support are now drawn in their actual working direction, not in positive direction. If only a first-order approach is used, reaction V_s is not used. Then the maximum bending moment is always located at the bottom or at the top of the web depending on the magnitude of H_s compared to M_s. If a second-order approach is used an additional bending moment in the web occurs equal to reaction V_s times the deflection in $x-$direction of the web. For this case, the position of the maximum bending moment depends on the reactions and the deflection of the web.

3.2 Rigid–plastic Behaviour

In the previous paragraph, an analytical model was presented to find the first location of yield of a hat-section strip dx, for different corner radii. If this location is known, a new analytical model can be developed which makes it possible to predict rigid-plastic strip behaviour. Figure 11 presents the geometry of the rigid-plastic model.

At the left of figure 11, the undeformed geometry is shown. Yield lines are shown by a bold dot. The yield line in the web has a distance L_y from the bottom of the web. This distance L_y depends on the corner radius and was predicted in the previous paragraph. Yield

lines are modelled at the bottom of the web and at the right in the top flange. The locations of these yield lines are according the observations of the finite element models in section two.

The displacement of the web u_1 and the upper part u_2 should be equal, therefore:

$$\begin{aligned} u_1 &= u_2 \Leftrightarrow -L_y \sin\varphi_a = \frac{b_{tf}}{2}(1-\cos\varphi_c) + (b_w - r - L_y)\sin\varphi_c \Leftrightarrow \\ \varphi_a &= \arcsin\left(\frac{\frac{b_{tf}}{2}(1-\cos\varphi_c) + (b_w - r - L_y)\sin\varphi_c}{-L_y}\right) \end{aligned} \tag{14}$$

The web crippling deformation Δh_w equals to the reduction of height of the two parts of the web and the top corner:

$$\Delta h_w = L_y(1-\cos\varphi_a) + (b_w - 2r - L_y)\,(1-\cos\varphi_c) - r\sin\varphi_c \tag{15}$$

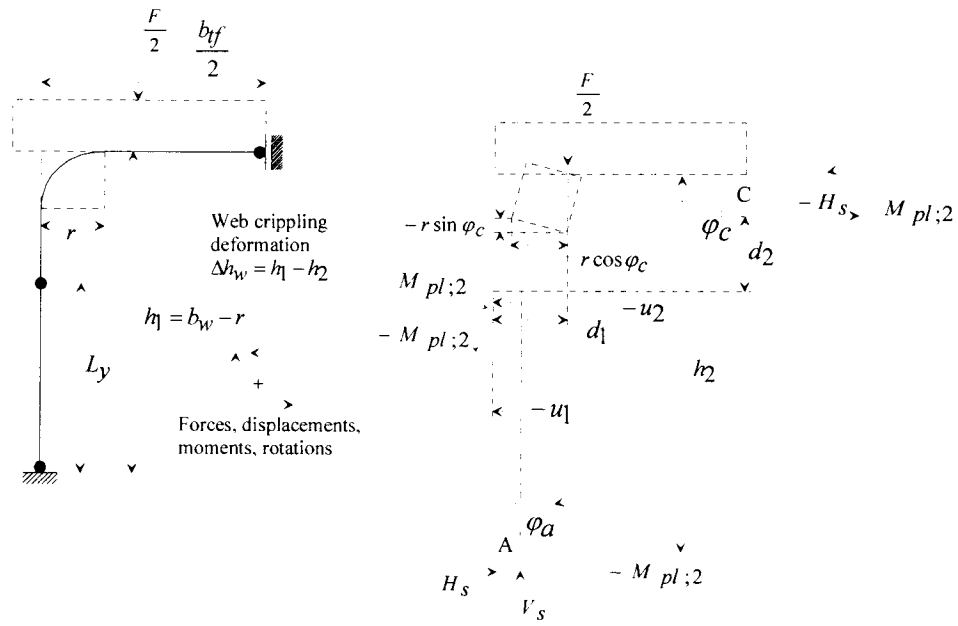

Figure 11: Detailed geometry to determine rigid-plastic behaviour.

The vertical reaction V_s at the bottom of the web equals the load $F/2$. At the yield line in the web, moment equilibrium exists for the lower part of the web:

$$M_{pl;2} - M_{pl;2} + H_s * L_y \cos\varphi_a + \frac{F}{2} * L_y \sin\varphi_a = 0 \tag{16}$$

At the yield line in the web, moment equilibrium exist for the upper part of the web, the top corner and top flange:

$$M_{pl;2} + M_{pl;2} - \frac{F}{2} * d_1 + H_s * d_2 = 0 \tag{17}$$

And:

$$d_1 = -(b_w - 2r - L_y)\sin\varphi_c + r\cos\varphi_c \tag{18}$$

$$d_2 = (b_w - r - L_y)\cos\varphi_c + \frac{b_{tf}}{2}\sin\varphi_c \tag{19}$$

The load F/2 can be solved from equations 16 and 17:

$$\frac{F}{2} = \frac{2(L_y M_{pl;2} + d_2 M_{pl;2}\sec\varphi_a)}{L_y(d_1 + d_2\tan\varphi_a)} \tag{20}$$

Using the yield strength f_y and steel plate thickness t, the plastic bending moment of a yield line equals:

$$M_{pl;2} = \frac{2}{\sqrt{3}} * \frac{1}{4} * t^2 * f_y * dx \tag{21}$$

A rigid-plastic curve of a strip dx can be calculated as follows. A rotation φ_c is taken. Then rotation φ_a can be calculated by equation 14 and the web crippling deformation Δh_w by equation 15. A fixed value for the distance L_y can be taken from the analytical model of paragraph 3.1. Nevertheless, it is also possible, for the web crippling deformation Δh_w, to find the distance L_y in the curves of figure 9. Both results are presented in figure 12. Because equation 14 and 15 are dependent on the value of distance L_y, these equations should be solved iterative using the curves of figure 9. Equation 20 calculates the load ($F/2$). Figure 12 presents rigid-plastic curves (bold lines) including the results of the finite element models (normal lines) for r=1, 10, and 15 mm. The results for r=3 mm and r=5 mm are almost equal to the results for r=1 mm. The dotted lines represent the same calculation as the normal rigid-plastic line, only the distance Ly has been fixed on its initial value.

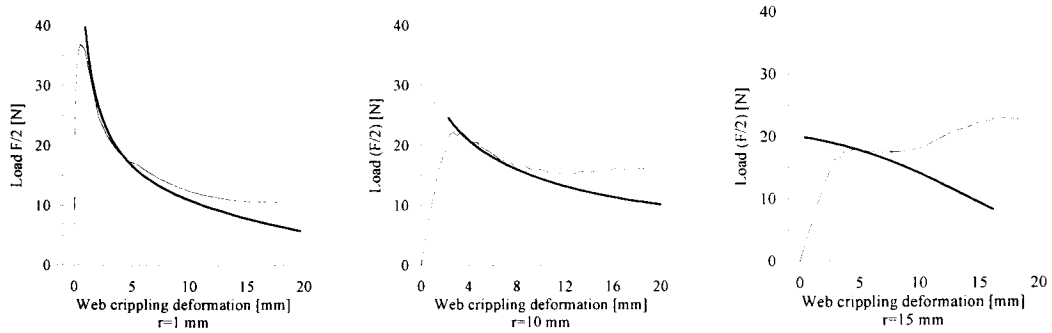

Fig. 12: Normal line: finite element model. Bold line: analytical model with moving yield line. Dotted line: analytical model. Dotted and dashed line: already existing analytical model for the rolling mechanism [1].

Especially the strips with small corner radii show an extremely close correlation between the analytical model and the finite element model. For large corner radii, r=15 mm, the rigid-plastic curve only joins the finite element model around the mechanism initiation load. This means the rigid-plastic behaviour of the strip dx for a corner radius r=15 mm is not correctly described by the analytical model, despite of the fact that the analytical model has no geometrical simplifications. One possible cause can be that strong deformations of the relatively weak corner radius lead to a different geometry, which seriously influences the load-deformation behaviour. Indeed, numerical analyses show that the corner radius deforms during the load-deformation path.

Another cause can be the movement of the yield line in the web. The movement of the yield line in the web dissipates energy, which is not taken into account in the analytical model. This should lead to an increasing underestimation of the rigid-plastic load for larger deformations, if yield line movement is strong (this is the case for large corner radii).

3.3 Existing Model for Rolling Mechanism

Bakker developed an analytical model for the rolling mechanism in 1992 [1]. A part of this model is shown in figure 13. This part of the model predicts the ultimate load for a small strip having three yield lines: two moving yield lines near the corner and one fixed yield line at the bottom of the web. The energy dissipated by the movement of the yield lines is taken into account.

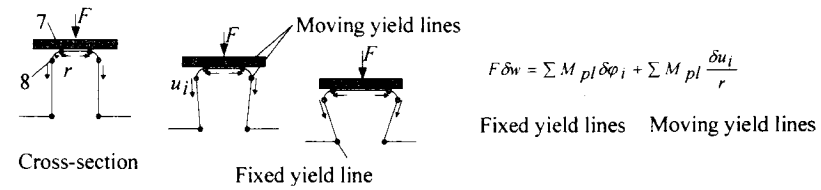

Figure 13: Analytical model for the rolling mechanism.

4. Discussion

4.1 Comparison of Analytical Models

In paragraph 3.2, an new analytical model was presented to predict the rigid-plastic behaviour for the strips. For r=15 mm, this model was not able to predict the curve of the finite element model correctly. Therefore, the already existing analytical model, in paragraph 3.3, for the rolling mechanism was tried. Note that this model takes the dissipated energy due to yield line movement into account.

Figure 12 shows that for a strip with r = 15 mm, also the existing model only predicts a part of the curve of the finite element model well. This means that the lack of modelling the energy dissipation for moving yield lines of the new model is not the cause for differences between the new model and the numerical simulations.

Figure 12 shows also that for a strip with r = 10 mm, a rolling mechanism does not occur because the model for the rolling mechanism predicts to high loads. For a hat-section with r = 10 mm, a rolling mechanism does occur.

4.2 Comparison of Strips and Whole Hat Sections Using Finite Element Models

A finite element model for a real hat-section with $r = 3\,\text{mm}$ was studied. This is shown in figure 14. After elastic behaviour, yield lines occur in the top flange near the corner and in the web between the middle of the web and the top corner. After some web crippling deformation, the yield line in the top flange stops rotating and the yield line in the web rotates further and moves slowly down in the web. Finally, a yield line occurs at the bottom of the strip. A strip with $r = 3\,\text{mm}$ behaves almost in the same manner as the real section. After elastic behaviour, it shows a yield line in the web, but not in the top flange. The line in the web is located a little bit lower than for the real hat-section. After some web crippling deformation, the yield line in the web moves slowly down in the web. Finally, yield lines occur at the bottom of the web and in the middle of the top flange.

Also a finite element model for a real hat-section with $r = 10\,\text{mm}$ was studied, figure 14. After elastic behaviour, two yield lines occur near the top corner: one in the web and one in the top flange. For more web crippling deformation, the yield line in the web moves strongly down through the web and the yield line in the top flange moves through the corner. Finally, a yield line occurs at the bottom of the web and in the middle of the top flange. A strip with $r = 10\,\text{mm}$ behaves equal to a strip with $r = 3\,\text{mm}$ (see previous paragraph). As additional information, it is interesting to observe that a strip with $r = 15\,\text{mm}$ has some more similarity with a hat-section with $r = 10\,\text{mm}$. After the forming of yield lines in the web, bottom of the strip, and in the top flange, a yield line occurs in the top corner too.

5. Conclusions and Further Research

For three-point bending tests of hat sections, the location of the first yield line in the web depends on the failure mechanism. For a rolling mechanism, the first yield line occurs in the web near the top corner and for a yield-arc mechanism, the first yield line occurs in the upper middle of the web. The analytical model for a strip dx of the hat section, explains these different yield line locations. Only one analytical model was used to show this for both mechanisms. A second-order calculation is necessary to predict the location of the first yield-line in the web.

For the finite element models of the strips dx, for intermediate corner radii, behaviour occurs that is a transition between the behaviour for large corner radii and small corner radii. This is not only seen for the load deformation behaviour, but also for the location and movement of the first yield line. As a conclusion, the strips dx do not fail by two completely different failure mechanisms. This was also observed for three-point bending tests [1], where sometimes a failure occurred which was a mixture of yield-arc and rolling failure.

An analytical model has been developed to find the rigid-plastic curves for the finite element models of the strips dx. Only one model was used. The model predicts the rigid-plastic curve of the strips well for r =1, 3, 5, and 10 mm. For the large corner radius $r = 15\,\text{mm}$ only a small part of the curve is covered. This is not caused by the lack of modelling the energy dissipation of the moving yield line in the web.

For small corner radii, the behaviour of a strip of a hat-section's cross-section is qualitatively similar to the behaviour of a real hat-section in a three-point bending test. For $r =$

10 mm, this is not the case (comparisons made based on finite element analyses and existing rolling model).

For a large corner radius, $r = 15\,\text{mm}$, an already existing analytical model for the rolling mechanism predicts the first part of the rigid-plastic curve well. The finite element model shows that for a strip with $r = 15\,\text{mm}$, two yield lines occur near the top corner. This makes it possible that for a strip with $r = 15\,\text{mm}$, indeed a rolling mechanism occurs. This needs further investigation.

Further research can be focussed on three items. First, boundary conditions of the strips can be studied for large corner radii. In this way, an explanation can be found for the different behaviour between strips and three-point bending tests. Secondly, for small corner radii, it can be investigated how the strip behaviour can be translated into behaviour of three-point bending tests. As a third item, inclined webs should be covered by the analytical models.

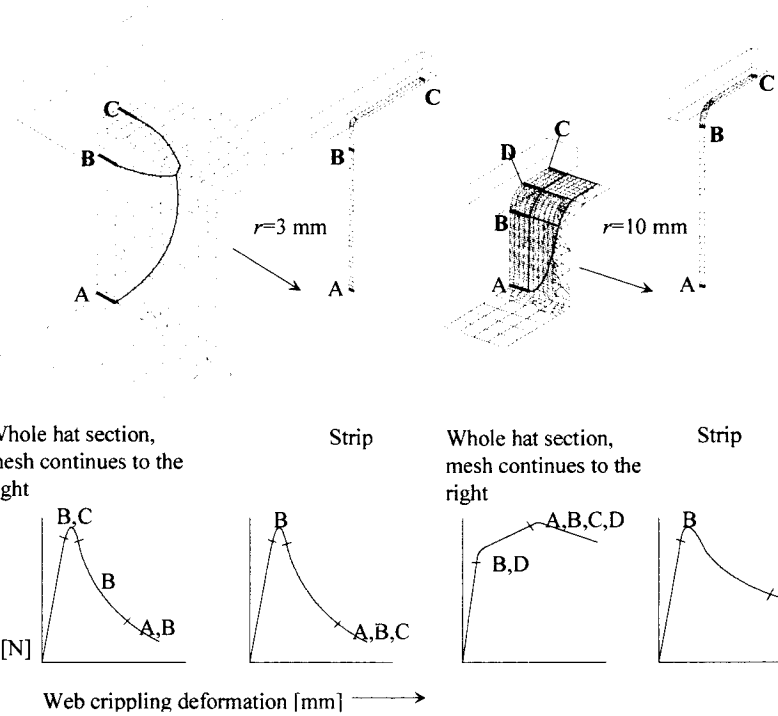

Figure 14: Behaviour of whole hat sections and strips for r =3 mm and r = 10 mm.

Acknowledgement

This research is supported by the Technology Foundation STW, applied science division of NWO and the technology programme of the Ministry of Economic Affairs.

References

[1] BAKKER, M. C. M.: *Web crippling of cold-formed steel sections.* Dissertation Eindhoven University of Technology, The Netherlands, 1992.

[2] HOFMEYER, H. - KERSTENS, J. G. M. - SNIJDER, H. H. - BAKKER, M. C. M.: *Research on the Behaviour of Combined Web Crippling and Bending of Steel Deck Sections*, published at the 13th International Speciality Conference on Cold-Formed Steel Structures, St. Louis, Missouri, U.S.A., October 18-19, 1996.

[3] TIMOSHENKO, S.: *Theory of Elastic Stability. Engineering Societies Monographs.* McGraw-Hill Book Company, New York and London, First edition, 1936.

[4] HILL, R.: *The Mathematical Theory of Plasticity*, London, Oxford University Press, 1950.

Received: 1999.06.15

H. Hofmeyer,
J. G. M. Kerstens,
H. H. Snijder,
M. C. M. Bakker,
Eindhoven University of Technology,
Faculty of Architecture Building and Planning,
Department of Structural Design,
Eindhoven, The Netherlands

H. H. Snijder,
Holland Railconsult,
Utrecht, The Netherlands

CONSTANT AMPLITUDE FATIGUE LIMIT FOR RIVETED GIRDERS

R. CROCETTI, M. AL-EMRANI, B. AKESSON, B. EDLUND

Key words: Riveted Girders, Fatigue, Clamping Force, Steel Bridges, Fatigue Damage Accumulation, Full-scale Fatigue Testing.

A fundamental topic regarding riveted structures subjected to dynamic loading, such as bridges, is the determination of the Constant Amplitude Fatigue Limit (CAFL). In order to gain an estimation of this limit, some 16 full-scale tests on stringers taken from an old railway bridge have been performed at the Department of Structural Engineering, Chalmers University of Technology. In order to reduce the extremely long time that this kind of experiments require, a technique, which is believed to be original, is proposed.

1. Introduction

The problem of keeping old railway bridges in service as long as possible is becoming an issue of more and more concern. This is primarily due to two reasons, namely:

- financial interest of the bridge owners;
- the inestimable cultural heritage represented by many bridges of this kind.

An adequate estimation of the remaining fatigue life of a riveted structure has often been impeded because of the insufficiency of a reasonable database of test results of full-size members. Even though considerable amount of fatigue testing on riveted structures has been carried out in Europe and North America during the past decade, there is still a lack of information in the region close to the CAFL. This region is of crucial importance, especially for the determination of whether or not previous dynamic loading (i.e. train passages) has produced fatigue damages.

2. Constant Amplitude Fatigue Limit for Riveted Bridges

The constant amplitude fatigue limit is defined as the stress range level below which there will be no fatigue crack growth during cyclic loading. A review of previously executed fatigue tests on rivet members by several researchers (see [2], for instance) indicates that this limit should – if it exists – fall within the stress amplitude range of 40-70 MPa. In order to achieve a more precise estimation about the CAFL, more tests are required within the above